HHS Public Access

Author manuscript

ACS Nano. Author manuscript; available in PMC 2022 November 11.

Published in final edited form as:

ACS Nano. 2021 July 27; 15(7): 11880–11890. doi:10.1021/acsnano.1c02982.

Liposomal Extravasation and Accumulation in Tumors as Studied by Fluorescence Microscopy and Imaging Depend on the Fluorescent Label

Guankui Wang[#],
Translational Bio-Nanosciences Laboratory, Department of Pharmaceutical Sciences, Skaggs School of Pharmacy and Pharmaceutical Sciences, and Colorado Center for Nanomedicine and Nanosafety, University of Colorado, Aurora, Colorado 80045, United States

Markella Zannikou[#],
Department of Neurological Surgery, Feinberg School of Medicine, Northwestern University, Chicago, Illinois 60611, United States

Laren Lofchy,
Translational Bio-Nanosciences Laboratory and Department of Pharmaceutical Sciences, Skaggs School of Pharmacy and Pharmaceutical Sciences, University of Colorado, Aurora, Colorado 80045, United States

Yue Li,
Translational Bio-Nanosciences Laboratory and Department of Pharmaceutical Sciences, Skaggs School of Pharmacy and Pharmaceutical Sciences, University of Colorado, Aurora, Colorado 80045, United States

Hanmant Gaikwad,
Translational Bio-Nanosciences Laboratory, Department of Pharmaceutical Sciences, Skaggs School of Pharmacy and Pharmaceutical Sciences, and Colorado Center for Nanomedicine and Nanosafety, University of Colorado, Aurora, Colorado 80045, United States

Irina V. Balyasnikova,
Department of Neurological Surgery, Feinberg School of Medicine and Northwestern Medicine Malnati Brain Tumor Institute of the Lurie Comprehensive Cancer Center, Feinberg School of Medicine, Northwestern University, Chicago, Illinois 60611, United States

Corresponding Authors Irina V. Balyasnikova, Dmitri Simberg.

[#]Author Contributions
G.W. and M.Z. contributed equally.

The authors declare no competing financial interest.

ASSOCIATED CONTENT
Supporting Information
The Supporting Information is available free of charge at https://pubs.acs.org/doi/10.1021/acsnano.1c02982.
Figure S1, images of EPC/DSPE-PEG2000/DiI/Cy5-DSPE liposomes in 4T1 tumor slices with lectin stained blood vessels and control tumor without liposomes; Figure S2, calibration of confocal microscope channel histogram prior to imaging of tumors; Figure S3, Images of EPC/DSPE-PEG2000/DiI/Cy5-DSPE liposomes in LY2 tumor slices with lectin stained blood vessels; Figure S4, images of HSPC/Chol/DSPE-PEG2000/DiI/Cy5-DSPE liposomes in 4T1 tumor; Figure S5, images of GL261 glioma slices without liposomes but with lectin stained blood vessels; Figure S6, plasma and blood cell fluorescence after injection of EPC/DSPE-PEG2000/DiI/Cy5-DSPE liposomes in 4T1 tumor bearing mice (for Figure 5C) (PDF)

Dmitri Simberg
Translational Bio-Nanosciences Laboratory, Department of Pharmaceutical Sciences, Skaggs School of Pharmacy and Pharmaceutical Sciences, and Colorado Center for Nanomedicine and Nanosafety, University of Colorado, Aurora, Colorado 80045, United States

Abstract

Tumor trafficking of liposomes is routinely monitored via fluorescence microscopy and imaging. To investigate whether an accumulation of liposomes depends on the type of fluorescent label, we prepared PEGylated liposomes dual-labeled with indocarbocyanine lipids (ICLs: DiD or DiI) and fluorescent phospholipids (FPLs: Cy3-DSPE or Cy5-DSPE) with similar cyanine headgroups but different spectra. Using *ex vivo* confocal microscopy and imaging, we compared tumor extravasation and accumulation of ICLs and FPLs. After systemic injection in a syngeneic mouse model of 4T1 breast cancer, ICLs and FPLs initially colocalized in tumor blood vessels and perivascular space. At later time points, ICLs spread over a significantly larger tumor area and accumulated in tumor macrophages, whereas FPLs were mostly restricted to the vasculature with limited extravascular signal. This phenomenon was independent of liposomal composition and ICL/FPL type and was also observed in syngeneic intracranial GL261 glioma and LY2 head and neck cancer models. The dual-labeled liposomes were stable in plasma and delivered both dyes to tumors at early time points. Notably, while the level of ICLs increased over time, FPLs gradually disappeared from tumors and other organs *in vivo*, likely due to degradation of the phospholipid. These findings demonstrate that trafficking and stability of the label is of critical importance when assessing extravasation and accumulation of nanocarriers in tumors and other organs by fluorescence microscopy and imaging.

Graphical Abstract

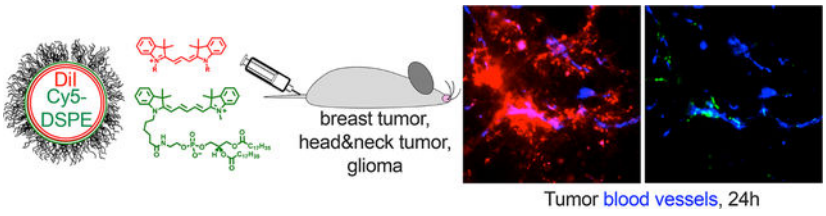

Keywords

liposome; confocal microscopy; fluorescence; extravasation; endothelium; lipids

Liposomes are the most adopted nanosized drug carriers that comprise over 30% of all nanopharmaceuticals currently in clinical trials.[1] The self-assembling property, the ability to encapsulate water-soluble and lipophilic drugs, scalability, well-characterized pharmacokinetics, and biodegradability make liposomes a popular choice of therapeutic carriers. The mechanisms whereby systemically injected liposomes accumulate in tumors are not clear. In the 1980s, Maeda reported the accumulation of macromolecules in tumors (termed the enhanced permeability-retention (EPR) effect).[2] Tumor permeability to nanoparticles is increased in response to inflammatory mediators histamine, bradykinin, C5a, or vascular growth factors.[3,4] The notion of pore transport as the primary mechanism

for the extravasation was indirectly suggested by the presence of gaps of irregular sizes between tumor endothelial cells in mouse models.[5] Endothelial gaps were also observed in nontumor blood vessels in response to the inflammatory mediators.[6] On the other hand, several publications suggested transendothelial migration of liposomes and nanoparticles,[7–9] likely to be mediated by vesiculo-vacuolar organelles,[10] and caveolae.[8,11,12] Regardless of the extravasation pathway, once liposomes and nanoparticles cross the endothelial barrier, the subsequent binding to the extracellular matrix and stroma and uptake by immune and tumor cells are critical for efficient retention in tumors.[13,14]

An overwhelming majority of studies on tumoral EPR effect of nanoparticles and liposomes employ fluorescence imaging and microscopy. These studies established the critical role of the nanoparticle size and geometry, physicochemical properties, tumor model, vascularization, and stage.[15–19] However, fluorescence imaging of tumors is often misleading due to quenching and tissue absorption of light outside of the optical window (650–900 nm).[20] We wondered, however, if the type of label also affects the tumoral extravasation and accumulation of liposomes as studied by fluorescence imaging and microscopy. Indocarbocyanine lipids (ICLs) are very popular lipophilic fluorescent dyes for labeling liposomes and nanoparticles.[21–24] as well as for long-term tracking of cells.[25–28] ICLs are stable in membranes and exhibit minimal transfer and exchange in serum,[29–31] possibly due to the highly lipophilic nature and mild cationic charge.[32] Headgroup-modified fluorescent phospholipids (FPLs), for example, lissamine rhodamine phosphatidylethanolamine, are another type of popular lipophilic dye used for liposomal labeling.[33–35] To our knowledge, tumoral accumulation and distribution of these two classes of dyes have not been compared side by side.

Here, we prepared liposomes that were double-labeled with dioctadecyl ICLs (C18-DiI or C18-DiD) and distearoyl FPLs (Cy5-DSPE or Cy3-DSPE). These fluorophores have long C18 alkyl or acyl chains to enable stable retention in liposomes and similar cyanine fluorophore headgroups (DiI is the dioctadecyl derivative of Cy3 and DiD is the dioctadecyl derivative of Cy5). To allow side-by-side comparison and to exclude the effect of size, charge, and composition of liposomes, both ICL and FPL were incorporated in the same liposome. We compared the extravasation and accumulation of the dyes in biologically relevant, syngeneic immunocompetent tumor models by *ex vivo* confocal microscopy and *ex vivo* imaging. We found that ICLs and FPLs accumulated in tumor blood vessels and extravasated to the same extent at early time points, but there was a much better migration and retention of ICLs at late time points. Unlike ICLs, we observed clearance of FPLs from tumors and other organs. The data suggest that trafficking and stability of fluorescent dyes is an important factor that could affect the conclusions about the magnitude of the EPR effect and long-term accumulation of liposomes in tumors and other organs.

RESULTS AND DISCUSSION

Liposomal ICLs and FPLs Show Similar Accumulation in Tumors at Early Time Points but Drastic Differences at Late Time Points.

To compare tumor accumulation and extravasation of DiI and a phospholipid with a similar cyanine fluorophore headgroup but different excitation/emission spectra, we synthesized

Cy5-DSPE (Figure 1A). We prepared 130 nm, negatively charged egg phosphatidylcholine (EPC)/DSPE-PEG2000 liposomes with 0.2 mol % of DiI and 0.2 mol % of Cy5-DSPE in the same liposome (Table 1). High-magnification confocal microscopy confirmed colocalization of both dyes in the same liposome, although the distribution of the dyes was not entirely homogeneous (Figure 1B). The liposomes were injected intravenously (i.v.) in 4T1 syngeneic orthotopic breast carcinoma-bearing mice. Confocal imaging of freshly excised (nonfixed to avoid dye migration[36]) tumor slices showed colocalization of both dyes in blood vessels at 1 h (Figure 1C, upper panel, Figure 1D, and Figure S1). However, at 24 h postinjection DiI efficiently extravasated and migrated throughout the tumor, whereas Cy5-DSPE mainly was confined to blood vessels (Figure 1C, lower panel, Figure 1D, and Figure S1). Quantification of confocal images taken in different areas of the tumor (gain settings were adjusted as described in the Methods and Figure S2) showed that while DiI and Cy5-DSPE occupied similar areas at 1 h postinjection, DiI occupied a significantly larger area than Cy5-DSPE at 4, 24, and 48 h postinjection (Figure 1E, p-value <0.0001 for all). To test another immunocompetent subcutaneous model, we injected DiI/Cy5-DSPE-labeled EPC/DSPE-PEG2000 liposomes in LY2 head and neck cancer, and again observed colocalization of DiI and Cy5-DSPE in blood vessels at 1 h postinjection and much better extravasation of DiI that Cy5-DSPE at 24 h (Figure S3).

Glioblastoma is the most aggressive and predominant type of gliomas with historical survival of only 20 months.[37,38] One of the main limitations of the current therapies is the insufficient delivery of drugs to tumors due to low penetration through the blood–brain barrier (BBB) and blood–tumor barrier (BTB).[39–41] Accumulation of nanoparticles in gliomas is often analyzed *via* imaging of ICL-labeled nanoparticles.[42] We injected EPC/DSPE-PEG2000 liposomes labeled with 0.2% DiI and 0.2% Cy5-DSPE i.v. in mice with syngeneic intracranial GL261 glioma model. At 48 h postinjection, mice were perfused with FITC-lectin (blood vessel label) and Hoechst (nuclear label). According to *ex vivo* confocal microscopy of fresh brain slices (the settings were adjusted as described in the Methods), DiI accumulated and spread in tumors much more efficiently than Cy5-DSPE (Figure 1F,G). DiI visibly extravasated the lectin-positive tumor blood vessels and spread over a much larger area than Cy5-DSPE (Figure 1F,G, p-value <0.0001).

We switched colors in the liposome to confirm that the observed difference is not fluorophore-dependent and is not due to a selective quenching of Cy5-DSPE in tumors. We synthesized Cy3-DSPE and coformulated it with DiD (Figure 2A) at 0.2% each in ~290 nm EPC/DSPE-PEG2000 liposomes (Table 1). Both dyes showed colocalization in liposomes under a high-magnification objective (Figure 2B). After 2–4 h i.v. injection in 4T1 tumor-bearing mice, DiD extravasated and migrated over a significantly larger area than Cy3-DSPE, which mostly stayed in blood vessels (Figure 2C,D, p-value <0.0001).

The experiments clearly demonstrate that ICLs and FPLs exhibit significant differences in tumor extravasation and distribution at late time points. To validate these findings for other liposomal compositions, we prepared 150 nm negatively charged HSPC/Chol/DSPE-PEG2000 liposomes (DOXIL formula, Table 1) labeled with both 0.2% DiI and 0.2% Cy5-DSPE and injected i.v. in 4T1 mice. Confocal microscopy at 24 h showed the same result

as for EPC/DSPE-PEG2000 liposomes, that is, more efficient extravasation and spreading of DiI than Cy5-DSPE (Figure S4).

Previous observations demonstrated that nanoparticles and liposomes accumulate in the immune microenvironment of tumors.[13,43] In some areas of 4T1 tumors, we did observe a macrophage-like accumulation pattern of lipids (not shown). To measure accumulation in immune cells, we prepared liposomes separately labeled with 0.2% DiD or Cy5-DSPE (Figure 3A and Table 1). Flow cytometry analysis 72 h after a single i.v. injection in 4T1 mice demonstrated minimal accumulation of Cy5-DSPE in cells in the tumor, whereas DiD liposomes resulted in about 17% of labeled cells (Figure 3B), with over 50% of F4/80+ tumor-associated macrophages being positive (Figure 3C,D). While it does not take into account the extracellular liposomes, the flow cytometry experiment demonstrated a much more efficient accumulation of ICLs than FPLs in tumor macrophages.

To characterize the immune uptake of ICLs in gliomas by immunostaining, we injected mice with liposomes labeled with a fixable DiI-amine (Figure 4A and Table 1). ICLs are nonfixable and migrate in tissues,[36] hence the need in the aminated ICL. Histological sections of GL261 tumors 48 h postinjection (Figure 4B) showed colocalization of DiI-amine with CD11b (myeloid) and CD45 (myeloid and lymphoid). Some proportion of DiI+ cells was negative for the immune markers. Overall, these findings suggest that ICLs are taken up by many populations of immune and nonimmune cells in tumors.

ICLs and FPLs Are Stable in Serum and Extravasate Together in Tumors but Show Differences in Stability in Tumors and Tissues.

Intrigued by these findings, we further investigated the fluorescence behavior of DiI/Cy5-DSPE-labeled EPC/DSPE-PEG2000 liposomes *in vitro* and *in vivo*. Both DiI and Cy5 fluorescence changed by less than 10% after incubation of liposomes in 1% Tween-20, suggesting low degree of quenching (Figure 5A). We next questioned if the observed differences between ICLs and FPLs are due to the differences in stability of the dyes in serum. Incubation of DiI/Cy5-DSPE liposomes in mouse serum showed less than 10% release of DiI and Cy5 fluorescence after 1 and 3 h (Figure 5B). Following injection in 4T1 bearing mice, the elimination profiles of Cy5-DSPE and DiI from plasma were similar in the first 60 min (Figure 5C, inset), but there was a faster elimination of Cy5-DSPE at 24 h (half-life 131 and 187 min, respectively). There was no binding of DiI/Cy5-DSPE liposomes to erythrocytes after injection *in vivo*, with over 99% of fluorescence associated with plasma (Figure S6). Confocal microscopy of liposomes in plasma 1 min and 1 h postinjection showed mostly intact DiI/Cy5-DSPE liposomes (Figure 5D). High-magnification confocal microscopy of 4T1 tumor cryosections 1 h postinjection showed intense binding of DiI/Cy5-DSPE liposomes to the tumor endothelium and initial extravasation of DiI and Cy5-DSPE (Figure 5E). These data demonstrate that liposomes are stable *in vivo* and bind to the tumor vasculature.

Since the accumulation of liposomes is often monitored *via ex vivo* organ imaging, we imaged DiI and Cy5 signals in excised tumors and livers at different time points postinjection (gain settings were adjusted as described in Methods). The tumor images (Figure 6A, upper panel) showed that both dyes accumulated to the same extent at 1 h. DiI

fluorescence continued to increase at 24 and 48 h, whereas Cy5 fluorescence plateaued at 24 h and dropped at 48 h (Figure 6A). A similar trend was observed for the liver images (Figure 6A, lower panel), which showed a similar accumulation of DiI and Cy5 signals at 1 h, but then an increase in DiI and a decrease in Cy5 at later time points. Measurement of the DiI/Cy5 fluorescence ratio in the images showed a ~6-fold increase over 48 h in both tumors and livers (Figure 6B). These data are consistent with the confocal imaging of tumors and suggest that in both tumors and livers, there is an initial accumulation of ICLs and FPLs, followed by a decrease of FPLs. Fluorescence lipids are known to undergo quenching in organs including liver;[44] therefore, we extracted the lipids from tumors, livers, spleens, and kidneys at 1, 24, and 48 h postinjection and remeasured the distribution (percent of injected dose/gram tissue) and DiI/Cy5 fluorescence ratio in the extracts. The organ distribution data in Figure 6C showed drastic differences in the tumor and organ accumulation between DiI and Cy5. Thus, while the DiI level showed an increase in all organs except kidney over 48 h, the Cy5 level did not show any increase or even decreased over time in all organs. The DiI/Cy5 fluorescence ratio over time showed a much higher increase in the liver and the spleen than in the tumor (Figure 6E).

The data above demonstrate that Cy5 fluorescence gradually disappears from the tumor and other tissues. This was especially prominent in the liver and spleen, which are the main organs that mediate the uptake of liposomes. To investigate whether Cy5 fluorescence is lost as a result of quenching or fluorophore metabolism, DiI/Cy5-DSPE liposomes were incubated in fresh liver homogenates for 1, 24, and 48 h. According to Figure 6E, there was no significant change in the DiI/Cy5 fluorescence ratio at all time points, suggesting no effect of the tissue homogenate on the fluorescence. A thin layer chromatography (TLC) analysis of extracts of the liver homogenates showed the presence of both dyes at 1 h. At 24 and 48 h, DiI was stable, whereas Cy5-DSPE showed degradation (Figure 6F). TLC analysis of the liver extracts of mice injected with DiI/Cy5-DSPE liposomes showed a degradation and disappearance of Cy5-DSPE, but not DiI at 24 and 48 h (Figure 6G), confirming that FPL is degraded and eliminated from the tissue.

The mechanism of the EPR effect of nanosized drug carriers is the fundamental question in drug delivery and is the subject of debate.[14] While fluorescent labels are commonly used to measure biodistribution and tumor accumulation of nanocarriers *in vivo* and in excised tumors *ex vivo*, fluorescence is highly problematic due to quenching and tissue absorbance,[44] and several publications stressed that radioactivity rather than fluorescence is the ultimate method for biodistribution measurements.[20,45,46] However, fluorescence microscopy and flow cytometry are indispensable for the assessment of nanocarrier extravasation and distribution in tumors. The labeling of liposomes is often based on lipophilic membrane dyes. The significance of this work is that using two main classes of fluorescent membrane dyes incorporated in the same PEGylated liposome, we demonstrated that depending on the label, a different conclusion can be made about the efficiency of the extravasation and accumulation in tumors as well as other organs. Thus, although ICL- and FPL-labeled liposomes showed efficient endothelial binding, likely due to the entrapment on a highly irregular surface of tumor vasculature, and similar extravasation efficiency of both dyes at early time points, ICLs exhibited significantly better extravasation, migration, and retention at later time points. While some of the liposomal formulations showed the

PDI larger than 0.2 and variability in terms of the surface charge, this is unlikely to affect the study's conclusion, since both ICL and FPL were coencapsulated at 1:1 molar ratio in the same liposome. The difference between ICLs and FPLs was observed regardless of the fluorophore wavelength, liposome type, and tumor type (breast, head and neck, and brain). The fluorescence properties and extinction coefficients of ICLs and FPLs are very similar due to the same class of fluorophore headgroup. Also, the intensity of the Cy3 and Cy5 channels was further calibrated using the liposomal batch used in each experiment. Collectively, the data suggest that the decrease in the FPL fluorescence in tumors is not due to a selective quenching of FPLs, but rather due to their degradation and elimination. This process is not specific to tumors and happens also in the liver, spleen, and kidneys. Once in the tissues, liposomal phospholipids could be subject to metabolism and degradation, most likely inside the cells, for example, by phospholipases,[47,48] as well as due to the acidic hydrolysis leading to a release of glycerol phosphoethanolamine and lysophospholipids.[49,50] FPLs could undergo the same fate, with smaller fluorescent fragments subsequently washed out of the tissues and the tumors. While LC-MS analysis of tissue extracts was not feasible due to a large excess of tissue lipids and hydrophobicity of ICLs and FPLs, TLC clearly demonstrated the degradation of FPLs in liver homogenates *in vitro* and liver extracts *in vivo*. A similar process likely happens in tumors. The uptake of liposomes and nanoparticles by the immune component of the tumors is well established,[13,43] and we observed the efficient uptake by tumor immune cells in both 4T1 and gliomas (Figures 3 and 4). The uptake by tumor macrophages could lead to degradation of FPLs in lysosomes while retaining a more stable ICLs.

CONCLUSIONS

In conclusion, our data suggest that the nature of the liposomal label could lead to differences in tumoral extravasation, trafficking and biodistribution as studied by microscopy and imaging. More studies are needed to further understand the impact of lipid structure in tumoral migration and uptake by the microenvironment. We recommend that caution should be exercised in interpreting biodistribution and tumor extravasation of nanocarriers based on indirect labeling.

METHODS

Materials.

DiD (1,1′-dioctadecyl-3,3,3′,3′-tetramethylindotricarbocyanine, 4-chlorobenzenesulfonate salt) and DiI (1,1′-dioctadecyl-3,3,3′,3′-tetramethylindotricarbocyanine perchlorate) were from Biotium (Hayward, CA, USA). Aminomethyl DiI was synthesized as described by us previously.[51] All fluorescent lipids were stored as 4–10 mM stock in ethanol. Whatman Nucleopore Track-Etch Membranes, bovine serum albumin, and the chemicals for FPL synthesis were from Sigma-Aldrich (St. Louis, MO, USA). Nitrocellulose membrane (0.45 μm) and PVDF membrane were from Bio-Rad (Hercules, CA, USA). Hydrogenated soy phosphatidylcholine, egg phosphatidylethanolamine, distearoyl phosphatidylethanolamine (DSPE), cholesterol, and DSPE-PEG2000 were from Avanti Polar Lipids (Alabaster, AL, USA) and were kept as chloroform stocks at −20 °C). Antimouse CD11b, antimouse

CD45, and antimouse F4/80 were from BioLegend (San Diego, CA, USA). Nuclear staining reagent Hoechst 33342 trihydrochloride trihydrate was purchased from Life Technologies (Carlsbad, CA, USA). Fetal bovine calf serum, RPMI 1640, and DMEM growth medium supplemented with L-glutamine were from Corning Inc. (New York, NY, USA). FITC-labeled tomato lectin (FL-1171–1) was from Vector Laboratories (Burlingame, CA, USA).

Synthesis of Cy5-DSPE and Cy3-DSPE.

A mixture of DSPE-NH_2 (8 mg, 0.01 mmol, 1 equiv) Cy5 NHS or Cy3-NHS (11.4 mg 0.015 mmol, 1.5 equiv) and DIEA (5.7 μL, 0.03 mmol, 3 equiv) was stirred in chloroform–methanol (9:1) at 50 °C for 2 h. The solvent was then evaporated under reduced pressure, and the resulting dark blue residue was purified by preparatory HPLC (C18 column) and eluted with 70% to 80% methanol/water (0.1% TFA), to obtain the product. The product was characterized by MALDI TOF mass spectrometry and was found to be 1212.77 Da for Cy5-DSPE and 1185.74 Da for Cy3-DSPE.

Liposome Preparation.

Lipids at the following molar ratios were mixed and dried under a nitrogen stream: HSPC/Chol/DSPE-PEG2000 (57/38/5) or EPC/DSPE-PEG2000 (95:5) with addition of 0.2% ICL and/or 0.2% FPL. The dry lipid cake was resuspended in PBS for a total lipid concentration of 20 mM and then incubated at 60 °C for 30 min. The solution was then vortexed for 2 min and bath sonicated. Liposomes were extruded by a syringe extruder (Avestin, Ottawa, Canada) through Whatman Nucleopore Track-Etch Membranes (200 nm pore size, 15 times). HSPC-based liposomes were extruded at 60 °C, EPC-based liposomes were extruded at room temperature. Size and ζ potential were measured at room temperature in 5% phosphate buffered saline using Zetasizer Nano (Malvern, UK). Liposomes were stored at 4 °C at a final concentration of 10 mM (total lipid) for a maximum period of 8 weeks before use.

Animal Experiments.

The University of Colorado and Northwestern University Institutional Animal Care and Use Committee (IACUC) approved animal experiments (protocols 103913(11) and IS00002999, respectively). The 4T1 cell line was purchased from the ATCC and verified using the University of Colorado sequencing core. LY2 cells derived from lymph node metastases that developed in BALB/c mice post-inoculation of PAM 212 squamous cell carcinoma cells were from Dr. Sana Karam, University of Colorado Anschutz Medical Campus. GL261 cells were obtained from the National Cancer Institute (NCI), and CT2A cells were a gift from Dr. Tom Seyfried (Boston College). Cells were grown at 37 °C in RPMI 1640 (4T1 cells), DMEM-F12 medium supplemented with 10% FBS and 1% primocin (LY2 cells), or DMEM (glioma cells) medium containing 10% heat-inactivated fetal bovine serum, 10 mM HEPES, 100 U/mL penicillin, and 100 ng/mL streptomycin (all from Corning Inc. New York, NY, USA). BALB/c mice of 8–10 weeks of age (females) were implanted with 0.5×10^6 4T1 cells into the mammary fat pad (4T1) or subcutaneously in the jaw region (LY2) and used for experiments 1 week later when tumors reached ~200–300 mm^3. For brain tumors, C57BL/6 mice (6–8 weeks old) were implanted with a total 1×10^5 GL261 or CT-2A cells per animal using an established protocol.[52] To determine the distribution of

liposomes in tumors and organs, liposomes were injected with 50 μL of 10 mM total lipid intravenously. Blood was collected *via* periorbital plexus using heparin glass capillaries, and the plasma was separated by centrifugation at 500*g* for 5 min. In some experiments, mice were preinjected before dissection with 50 μL of FITC-tomato lectin (1 mg/mL) and 50 μL Hoechst 33324 (2 mg/mL) to visualize the vasculature and the nuclei. Mice were sacrificed with carbon dioxide, followed by cardiac perfusion with PBS through the left ventricle.

Microscopy.

Nikon Eclipse AR1HD inverted confocal microscope with 405, 488, 561, and 640 nm excitation lasers and corresponding emission filters was used. For high-magnification imaging, liposomes were diluted 1:1000 in PBS, mixed with glycerol at 1:1 ratio, and 2 μL was placed on a slide and covered with a glass coverslip. For liposomes in plasma, the samples were diluted 1:100 (early time point) or 1:50 (late time point) and mixed with glycerol. The preparations in glycerol were spread under a coverslip and imaged under an Apo60 or Apo100 Oil objective at 2048 × 2048 resolution. For tumor imaging, tumors or whole brains were frozen on dry ice and sliced with a blade into 1–2 mm thick slices. The slices were placed on a glass slide and imaged using Plan Apo 10 objective. Channels' voltage and laser intensity were adjusted using the dual-labeled liposomes placed on a slide and imaged under the same magnification. These parameters were calibrated before each imaging session using the batch of liposomes used in that experiment. For quantification, multiple random image areas from different slices of the tumor (both periphery and center) were acquired at 512 × 512 resolution. Images were quantified with Fiji using built-in or customized macros. Briefly, 8-bit gray image stacks were automatically thresholded and the percentages of binary (positive) areas in the Cy3 and Cy5 channels were calculated using the "Measure" function. All the data were plotted with Prism version 8.3.0 (GraphPad, San Diego, CA).

Flow Cytometry and Immunostaining.

A single-cell suspension of tumor tissue was prepared for flow cytometry analysis, as previously described.[52] Single cell isolates were preblocked with Ultra-LEAF purified antimouse CD16/32 antibody (BioLegend, San Diego, CA) in PBS supplemented with 2% FBS 10 min at 4 °C before antibody staining. The 4T1 single-cell suspension was stained with anti-F4/80-AF488. After incubation on ice for 20 min and washing, cells were analyzed for staining using the cells were analyzed with Guava EasyCyte HT flow cytometer (Merck KGaA). Cells were resuspended at ~0.5 million/mL and 20 000 events were detected. Dead cells and microparticles were excluded with FSC/SSC and the percentage of Cy5+ cells was analyzed with FlowJo software Version 10.6 (FlowJo, LLC). For immunostaining, mice with GL261 tumors were injected with DiI-amine liposomes and perfused 48 h postinjection. Brains were snap-frozen in OCT in liquid nitrogen and sectioned with a cryostat into 5–8 μm sections. The sections were fixed with 4% formalin on a slide, blocked with 10% goat serum, and stained with anti-CD11b and CD45 antibodies and corresponding secondary antibodies.

Dye Stability in Serum and Liver Homogenates.

Liposomes were incubated at 2 mM in 80% mouse serum, PBS, or 1% Tween/PBS for different times at 37 °C. Following incubation, the samples were dotted on a nitrocellulose membrane and imaged at Cy3 and Cy5 wavelengths. Alternatively, to measure the release in serum, the samples were diluted after incubation 10-fold in PBS and ultra-centrifuged at 80 000 rpm for 30 min, 4 °C using TLA-100.3 rotor of Beckman Optima ultracentrifuge. The supernatant in serum, liposomes in whole serum and liposomes in PBS were dotted and scanned at Cy3 and Cy5 wavelengths with Bio-Rad camera imager using Cy3 and Cy5 filters. The mean fluorescence of the dots was determined and used to calculate the percentage of release in serum. To measure the effect of tissue on DiI/Cy5 fluorescence ratio, livers from BALB/c mice were homogenized for 5 min in PBS (1:2 weight: volume ratio) using BioSpec Mini BeadBeater-16 tissue homogenizer with 1–2 zirconium beads added per tube. Liposomes were added at a 1:10 ratio to the homogenate and incubated at 37 °C for different times. The homogenate was further diluted 10-fold, dotted on a nitrocellulose membrane, and scanned with Bio-Rad gel imager at Cy3 and Cy5 channels as described above.

Organ and Plasma Imaging.

Tumors and livers were placed in a 24-well plate and imaged with Bio-Rad imaged at Cy3 and Cy5 wavelengths. To match the intensity of the channels, the same liposomes used for injection were diluted (1:10), dotted on a 0.45 μm nitrocellulose membrane, and scanned together with the samples. Mean fluorescence was determined from 8-bit TIFF images using Fiji software by drawing a region of interest around the tumors and using the “Measure” function to determine mean gray values. Such measurement is independent of the organ cross-section area. The mean gray values of noninjected tumors were subtracted from the measurements. For elimination of DiI and Cy5-DSPE, blood was collected at different time points and separated into plasma and RBCs by centrifugation at 500*g* for 5 min. The RBC fraction was washed three times with PBS and brought to the original blood volume. Both plasma and RBC fractions were dotted on a nitrocellulose membrane. Standard dilutions of liposomes in noninjected plasma were also dotted, the membrane was scanned as above, and the %ID per gram plasma was calculated (assuming blood is 7% of mouse weight, and 50% hematocrit). The data were plotted with Prism, and the liposomal half-life was calculated using monoexponential decay curve fit.

Organ Extractions and Thin Layer Chromatography (TLC).

For extraction using a modified Bligh–Dyer method,[53] 50–100 mg of tissue was weighted and homogenized as described above. Ten parts of chloroform/methanol (2:1) were added to the homogenate (considering that organ homogenate is 1 part), and the samples were mixed at 1400 rpm for 2 h at room temperature on Eppendorf Thermomixer. The tubes were centrifuged at 500*g* for 10 min. The organic phase (bottom, approximately 80% of the added amount) was carefully collected, dotted as 2 μL aliquots on a PVDF membrane, and scanned for DiI and Cy5 fluorescence as described above. Dilutions of EPC/DSPE-PEG2000/DiI/Cy5 liposomes (standard curve) made in extracts of organs from noninjected mouse were dotted on the same membrane and scanned together with the samples. The

percent of the injected dose of DiI and Cy5 in the extracts was calculated and divided by the respective wet tissue weight. The fluorescence of control noninjected organs was subtracted from that of injected organs. For TLC analysis, the mobile phase consisted of chloroform: methanol (9:1) with 1% trifluoroacetic acid, and the samples were run on TLC Silica Gel 60 F254 (EMD Millipore).

Supplementary Material

Refer to Web version on PubMed Central for supplementary material.

ACKNOWLEDGMENTS

The study was supported by NIH grant R01CA194058 to D.S. and NIH grants R33NS101150, R01NS106379, and R01NS122395 to I.V.B.

REFERENCES

(1). D'Mello SR; Cruz CN; Chen ML; Kapoor M; Lee SL; Tyner KM The Evolving Landscape of Drug Products Containing Nanomaterials in the United States. Nat. Nanotechnol. 2017, 12, 523–529. [PubMed: 28436961]

(2). Matsumura Y; Maeda H A New Concept for Macromolecular Therapeutics in Cancer Chemotherapy: Mechanism of Tumoritropic Accumulation of Proteins and the Antitumor Agent Smancs. Cancer Res. 1986, 46, 6387–6392. [PubMed: 2946403]

(3). Monsky WL; Fukumura D; Gohongi T; Ancukiewcz M; Weich HA; Torchilin VP; Yuan F; Jain RK Augmentation of Transvascular Transport of Macromolecules and Nanoparticles in Tumors Using Vascular Endothelial Growth Factor. Cancer Res. 1999, 59, 4129–4135. [PubMed: 10463618]

(4). Tee JK; Yip LX; Tan ES; Santitewagun S; Prasath A; Ke PC; Ho HK; Leong DT Nanoparticles' Interactions with Vasculature in Diseases. Chem. Soc. Rev. 2019, 48, 5381–5407. [PubMed: 31495856]

(5). Hashizume H; Baluk P; Morikawa S; McLean JW; Thurston G; Roberge S; Jain RK; McDonald DM Openings between Defective Endothelial Cells Explain Tumor Vessel Leakiness. Am. J. Pathol. 2000, 156, 1363–1380. [PubMed: 10751361]

(6). Baluk P; Hirata A; Thurston G; Fujiwara T; Neal CR; Michel CC; McDonald DM Endothelial Gaps: Time Course of Formation and Closure in Inflamed Venules of Rats. Am. J. Physiol. 1997, 272, L155–L170. [PubMed: 9038915]

(7). Thurston G; McLean JW; Rizen M; Baluk P; Haskell A; Murphy TJ; Hanahan D; McDonald DM Cationic Liposomes Target Angiogenic Endothelial Cells in Tumors and Chronic Inflammation in Mice. J. Clin. Invest. 1998, 101, 1401–1413. [PubMed: 9525983]

(8). Liu X; Lin P; Perrett I; Lin J; Liao YP; Chang CH; Jiang J; Wu N; Donahue T; Wainberg Z; Nel AE; Meng H Tumor-Penetrating Peptide Enhances Transcytosis of Silicasome-Based Chemotherapy for Pancreatic Cancer. J. Clin. Invest. 2017, 127, 2007–2018. [PubMed: 28414297]

(9). Sindhwani S; Syed AM; Ngai J; Kingston BR; Maiorino L; Rothschild J; MacMillan P; Zhang Y; Rajesh NU; Hoang T; Wu JLY; Wilhelm S; Zilman A; Gadde S; Sulaiman A; Ouyang B; Lin Z; Wang L; Egeblad M; Chan WCW The Entry of Nanoparticles into Solid Tumours. Nat. Mater. 2020, 19, 566–575. [PubMed: 31932672]

(10). Dvorak AM; Kohn S; Morgan ES; Fox P; Nagy JA; Dvorak HF The Vesiculo-Vacuolar Organelle (VVO): A Distinct Endothelial Cell Structure That Provides a Transcellular Pathway for Macromolecular Extravasation. J. Leukocyte Biol. 1996, 59, 100–115. [PubMed: 8558058]

(11). Liu X; Jiang J; Meng H Transcytosis - an Effective Targeting Strategy That Is Complementary to "Epr Effect" for Pancreatic Cancer Nano Drug Delivery. Theranostics 2019, 9, 8018–8025. [PubMed: 31754378]

(12). Moghimi SM; Simberg D Nanoparticle Transport Pathways into Tumors. J. Nanopart. Res. 2018, 20, 169. [PubMed: 29950922]

(13). Korangath P; Barnett JD; Sharma A; Henderson ET; Stewart J; Yu SH; Kandala SK; Yang CT; Caserto JS; Hedayati M; Armstrong TD; Jaffee E; Gruettner C; Zhou XC; Fu W; Hu C; Sukumar S; Simons BW; Ivkov R Nanoparticle Interactions with Immune Cells Dominate Tumor Retention and Induce T Cell-Mediated Tumor Suppression in Models of Breast Cancer. Sci. Adv. 2020, 6, No. eaay1601.

(14). Anchordoquy TJ; Barenholz Y; Boraschi D; Chorny M; Decuzzi P; Dobrovolskaia MA; Farhangrazi ZS; Farrell D; Gabizon A; Ghandehari H; Godin B; La-Beck NM; Ljubimova J; Moghimi SM; Pagliaro L; Park JH; Peer D; Ruoslahti E; Serkova NJ; Simberg D Mechanisms and Barriers in Cancer Nanomedicine: Addressing Challenges, Looking for Solutions. ACS Nano 2017, 11, 12–18. [PubMed: 28068099]

(15). Toy R; Hayden E; Camann A; Berman Z; Vicente P; Tran E; Meyers J; Pansky J; Peiris PM; Wu H; Exner A; Wilson D; Ghaghada KB; Karathanasis E Multimodal *in Vivo* Imaging Exposes the Voyage of Nanoparticles in Tumor Microcirculation. ACS Nano 2013, 7, 3118–3129. [PubMed: 23464827]

(16). Stirland DL; Matsumoto Y; Toh K; Kataoka K; Bae YH Analyzing Spatiotemporal Distribution of Uniquely Fluorescent Nanoparticles in Xenograft Tumors. J. Controlled Release 2016, 227, 38–44.

(17). Smith BR; Kempen P; Bouley D; Xu A; Liu Z; Melosh N; Dai H; Sinclair R; Gambhir SS Shape Matters: Intravital Microscopy Reveals Surprising Geometrical Dependence for Nanoparticles in Tumor Models of Extravasation. Nano Lett. 2012, 12, 3369–3377. [PubMed: 22650417]

(18). Chauhan VP; Stylianopoulos T; Martin JD; Popovic Z; Chen O; Kamoun WS; Bawendi MG; Fukumura D; Jain RK Normalization of Tumour Blood Vessels Improves the Delivery of Nanomedicines in a Size-Dependent Manner. Nat. Nanotechnol. 2012, 7, 383–388. [PubMed: 22484912]

(19). Yuan F; Dellian M; Fukumura D; Leunig M; Berk DA; Torchilin VP; Jain RK Vascular Permeability in a Human Tumor Xenograft: Molecular Size Dependence and Cutoff Size. Cancer Res. 1995, 55, 3752–3756. [PubMed: 7641188]

(20). Deng H; Konopka CJ; Cross TL; Swanson KS; Dobrucki LW; Smith AM Multimodal Nanocarrier Probes Reveal Superior Biodistribution Quantification by Isotopic Analysis over Fluorescence. ACS Nano 2020, 14, 509–523. [PubMed: 31887006]

(21). Guo P; Liu D; Subramanyam K; Wang B; Yang J; Huang J; Auguste DT; Moses MA Nanoparticle Elasticity Directs Tumor Uptake. Nat. Commun. 2018, 9, 130. [PubMed: 29317633]

(22). Zhang Q; Lu L; Zhang L; Shi K; Cun X; Yang Y; Liu Y; Gao H; He Q Dual-Functionalized Liposomal Delivery System for Solid Tumors Based on RGD and a Ph-Responsive Antimicrobial Peptide. Sci. Rep. 2016, 6, 19800. [PubMed: 26842655]

(23). Syed AM; MacMillan P; Ngai J; Wilhelm S; Sindhwani S; Kingston BR; Wu JLY; Llano-Suarez P; Lin ZP; Ouyang B; Kahiel Z; Gadde S; Chan WCW Liposome Imaging in Optically Cleared Tissues. Nano Lett. 2020, 20, 1362–1369. [PubMed: 31928014]

(24). Beztsinna N; Tsvetkova Y; Bartneck M; Lammers T; Kiessling F; Bestel I Amphiphilic Phospholipid-Based Riboflavin Derivatives for Tumor Targeting Nanomedicines. Bioconjugate Chem. 2016, 27, 2048–2061.

(25). Progatzky F; Dallman MJ; Lo Celso C From Seeing to Believing: Labelling Strategies for *in Vivo* Cell-Tracking Experiments. Interface Focus 2013, 3, 20130001. [PubMed: 23853708]

(26). Zagorodnyuk VP; Kyloh M; Nicholas S; Peiris H; Brookes SJ; Chen BN; Spencer NJ Loss of Visceral Pain Following Colorectal Distension in an Endothelin-3 Deficient Mouse Model of Hirschsprung's Disease. J. Physiol. 2011, 589, 1691–1706. [PubMed: 21320883]

(27). Kalchenko V; Shivtiel S; Malina V; Lapid K; Haramati S; Lapidot T; Brill A; Harmelin A Use of Lipophilic Near-Infrared Dye in Whole-Body Optical Imaging of Hematopoietic Cell Homing. J. Biomed. Opt. 2006, 11, 050507. [PubMed: 17092148]

(28). Lo Celso C; Fleming HE; Wu JW; Zhao CX; Miake-Lye S; Fujisaki J; Cote D; Rowe DW; Lin CP; Scadden DT Live-Animal Tracking of Individual Haematopoietic Stem/Progenitor Cells in Their Niche. Nature 2009, 457, 92–96. [PubMed: 19052546]

(29). Bastiat G; Pritz CO; Roider C; Fouchet F; Lignieres E; Jesacher A; Glueckert R; Ritsch-Marte M; Schrott-Fischer A; Saulnier P; Benoit JP A New Tool to Ensure the Fluorescent Dye Labeling Stability of Nanocarriers: A Real Challenge for Fluorescence Imaging. J. Controlled Release 2013, 170, 334–342.

(30). Shi G; Mukthavaram R; Kesari S; Simberg D Distearoyl Anchor-Painted Erythrocytes with Prolonged Ligand Retention and Circulation Properties *in Vivo*. Adv. Healthcare Mater. 2014, 3, 142–148.

(31). Griffin JI; Wang G; Smith WJ; Vu VP; Scheinman R; Stitch D; Moldovan R; Moghimi SM; Simberg D Revealing Dynamics of Accumulation of Systemically Injected Liposomes in the Skin by Intravital Microscopy. ACS Nano 2017, 11, 11584–11593. [PubMed: 29045127]

(32). Gullapalli RR; Demirel MC; Butler PJ Molecular Dynamics Simulations of Dii-C18(3) in a Dppc Lipid Bilayer. Phys. Chem. Chem. Phys. 2008, 10, 3548–3560. [PubMed: 18548161]

(33). Li L; ten Hagen TL; Schipper D; Wijnberg TM; van Rhoon GC; Eggermont AM; Lindner LH; Koning GA Triggered Content Release from Optimized Stealth Thermosensitive Liposomes Using Mild Hyperthermia. J. Controlled Release 2010, 143, 274–279.

(34). Sriraman SK; Salzano G; Sarisozen C; Torchilin V Anti-Cancer Activity of Doxorubicin-Loaded Liposomes Co-Modified with Transferrin and Folic Acid. Eur. J. Pharm. Biopharm. 2016, 105, 40–49. [PubMed: 27264717]

(35). Nik ME; Malaekeh-Nikouei B; Amin M; Hatamipour M; Teymouri M; Sadeghnia HR; Iranshahi M; Jaafari MR Liposomal Formulation of Galbanic Acid Improved Therapeutic Efficacy of Pegylated Liposomal Doxorubicin in Mouse Colon Carcinoma. Sci. Rep. 2019, 9, 9527. [PubMed: 31267009]

(36). von Bartheld CS; Cunningham DE; Rubel EW Neuronal Tracing with Dii: Decalcification, Cryosectioning, and Photoconversion for Light and Electron Microscopic Analysis. J. Histochem. Cytochem. 1990, 38, 725–733. [PubMed: 2185313]

(37). Stupp R; Taillibert S; Kanner A; Read W; Steinberg D; Lhermitte B; Toms S; Idbaih A; Ahluwalia MS; Fink K; Di Meco F; Lieberman F; Zhu JJ; Stragliotto G; Tran D; Brem S; Hottinger A; Kirson ED; Lavy-Shahaf G; Weinberg U; et al. Effect of Tumor-Treating Fields Plus Maintenance Temozolomide *vs* Maintenance Temozolomide Alone on Survival in Patients with Glioblastoma: A Randomized Clinical Trial. JAMA 2017, 318, 2306–2316. [PubMed: 29260225]

(38). Hottinger AF; Pacheco P; Stupp R Tumor Treating Fields: A Novel Treatment Modality and Its Use in Brain Tumors. Neuro Oncol. 2016, 18, 1338–1349. [PubMed: 27664860]

(39). Krenciute G; Prinzing BL; Yi Z; Wu MF; Liu H; Dotti G; Balyasnikova IV; Gottschalk S Transgenic Expression of Il15 Improves Antiglioma Activity of Il13ralpha2-Car T Cells but Results in Antigen Loss Variants. Cancer Immunol. Res. 2017, 5, 571–581. [PubMed: 28550091]

(40). Pardridge WM The Blood-Brain Barrier: Bottleneck in Brain Drug Development. NeuroRx 2005, 2, 3–14. [PubMed: 15717053]

(41). Pitz MW; Desai A; Grossman SA; Blakeley JO Tissue Concentration of Systemically Administered Antineoplastic Agents in Human Brain Tumors. J. Neuro-Oncol. 2011, 104, 629–638.

(42). Shergalis A; Bankhead A 3rd; Luesakul U; Muangsin N; Neamati N Current Challenges and Opportunities in Treating Glioblastoma. Pharmacol. Rev. 2018, 70, 412–445. [PubMed: 29669750]

(43). Dai Q; Wilhelm S; Ding D; Syed AM; Sindhwani S; Zhang Y; Chen YY; MacMillan P; Chan WCW Quantifying the Ligand-Coated Nanoparticle Delivery to Cancer Cells in Solid Tumors. ACS Nano 2018, 12, 8423–8435. [PubMed: 30016073]

(44). Meng F; Wang J; Ping Q; Yeo Y Quantitative Assessment of Nanoparticle Biodistribution by Fluorescence Imaging, Revisited. ACS Nano 2018, 12, 6458–6468. [PubMed: 29920064]

(45). Glassman PM; Muzykantov VR Pharmacokinetic and Pharmacodynamic Properties of Drug Delivery Systems. J. Pharmacol. Exp. Ther. 2019, 370, 570–580. [PubMed: 30837281]

(46). Scherpereel A; Wiewrodt R; Christofidou-Solomidou M; Gervais R; Murciano JC; Albelda SM; Muzykantov VR Cell-Selective Intracellular Delivery of a Foreign Enzyme to Endothelium *in Vivo* Using Vascular Immunotargeting. FASEB J. 2001, 15, 416–426. [PubMed: 11156957]

(47). Mumtaz Virk M; Reimhult E Phospholipase A2-Induced Degradation and Release from Lipid-Containing Polymersomes. Langmuir 2018, 34, 395–405. [PubMed: 29231739]

(48). Hansen AH; Mouritsen OG; Arouri A Enzymatic Action of Phospholipase a(2) on Liposomal Drug Delivery Systems. Int. J. Pharm. 2015, 491, 49–57. [PubMed: 26056930]

(49). Grit M; Crommelin DJ The Effect of Surface Charge on the Hydrolysis Kinetics of Partially Hydrogenated Egg Phosphatidylcholine and Egg Phosphatidylglycerol in Aqueous Liposome Dispersions. Biochim. Biophys. Acta, Lipids Lipid Metab. 1993, 1167, 49–55.

(50). Grit M; Zuidam NJ; Underberg WJ; Crommelin DJ Hydrolysis of Partially Saturated Egg Phosphatidylcholine in Aqueous Liposome Dispersions and the Effect of Cholesterol Incorporation on Hydrolysis Kinetics. J. Pharm. Pharmacol. 2011, 45, 490–495.

(51). Smith WJ; Tran H; Griffin JI; Jones J; Vu VP; Nilewski L; Gianneschi N; Simberg D Lipophilic Indocarbocyanine Conjugates for Efficient Incorporation of Enzymes, Antibodies and Small Molecules into Biological Membranes. Biomaterials 2018, 161, 57–68. [PubMed: 29421563]

(52). Pituch KC; Miska J; Krenciute G; Panek WK; Li G; Rodriguez-Cruz T; Wu M; Han Y; Lesniak MS; Gottschalk S; Balyasnikova IV Adoptive Transfer of Il13ralpha2-Specific Chimeric Antigen Receptor T Cells Creates a Pro-Inflammatory Environment in Glioblastoma. Mol. Ther. 2018, 26, 986–995. [PubMed: 29503195]

(53). Bligh EG; Dyer WJ A Rapid Method of Total Lipid Extraction and Purification. Can. J. Biochem. Physiol. 1959, 37, 911–917. [PubMed: 13671378]

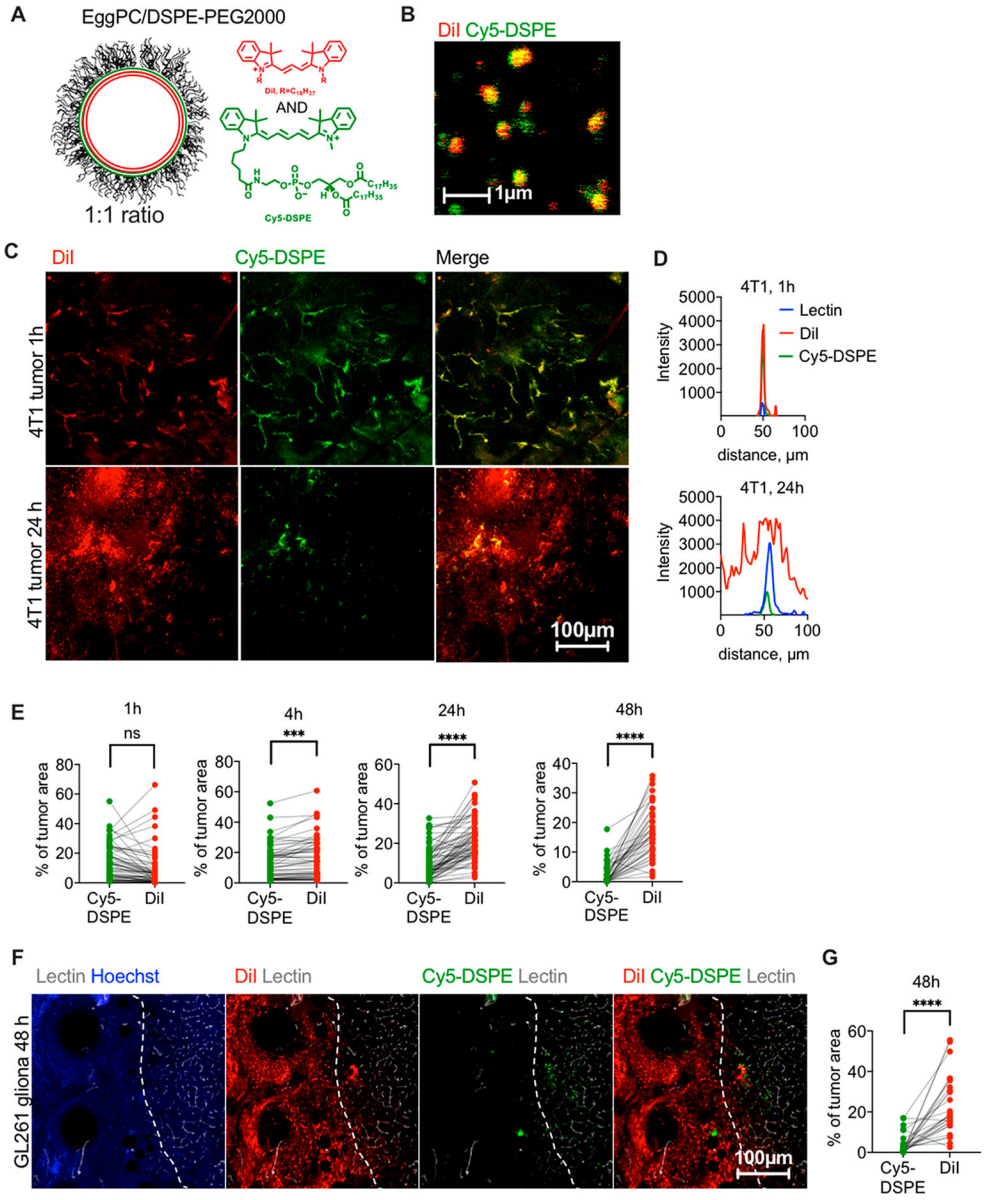

Figure 1.

ICLs exhibit enhanced extravasation in syngeneic solid tumors. (A) EPC/DSPE-PEG2000/DiI/Cy5-DSPE liposomes were used (Table 1). (B) both dyes are colocalized in liposomes. The size estimate by fluorescence microscopy is not accurate, and readers are referred to Table 1 for accurate size and PDI measurements. (C) Confocal microscopy imaging of fresh 4T1 tumor slices shows colocalization of DiI and Cy5-DSPE in tumor vasculature but predominant extravasation and spreading of DiI at 24 h. (D) Line profiles drawn across representative lectin-labeled tumor blood vessels (Figure S1) show spreading of DiI at 24 h and mostly vascular localization of Cy5-DSPE. (E) Quantification of fluorescence positive areas in the tumor (n = 30–60 images from 2 tumors per time point, paired t test, repeated twice). (F)EPC/DSPE-PEG2000/DiI/Cy5-DSPE liposomes were injected in GL261 syngeneic intracranial glioma bearing mice. Confocal microscopy

imaging of brain slices shows predominant extravasation and spreading of DiI, and an almost complete absence of Cy5-DSPE. The tumor (left of dotted boundary as identified by highly irregular tumor blood vessels) is surrounded by normal brain tissue with defined vasculature. (G) Quantification of fluorescence-positive areas in the glioma images ($n = 40$ images from 2 tumors, paired t test).

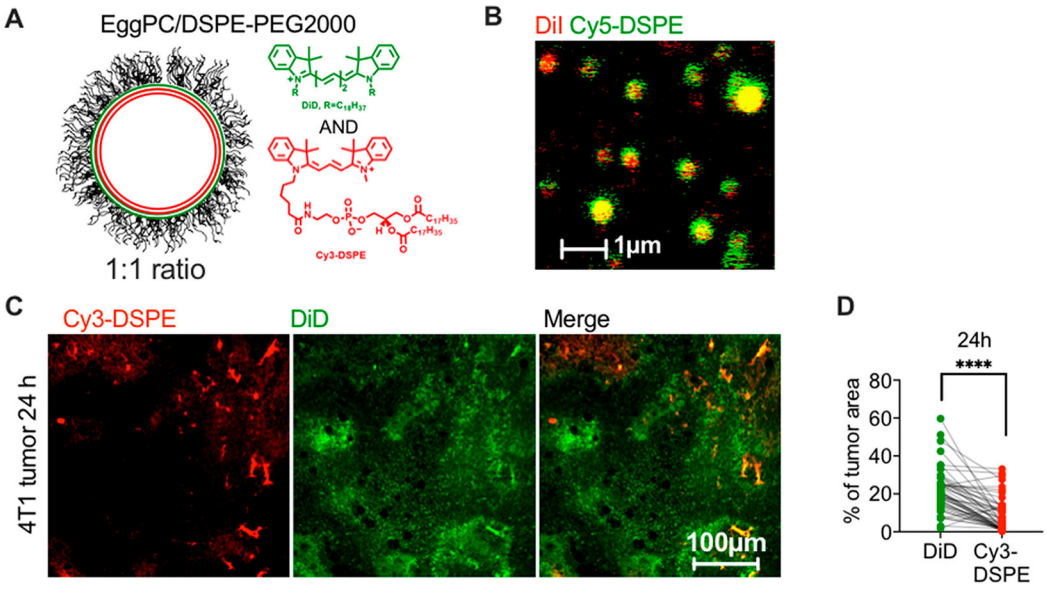

Figure 2.

The switch of fluorophore does not affect the enhanced extravasation of ICLs over FPLs. (A) EPC/DSPE-PEG2000/DiD/Cy3-DSPE liposomes were used (Table 1). (B) Both dyes showed colocalization in liposomes. Note that the size estimate by fluorescence microscopy is not accurate, and readers are referred to Table 1 for accurate size and PDI measurements. (C) Confocal images of tumor slices and (D) image area quantification show predominant spreading of DiD in tumors (n = 60 images from 3 mice, paired t test).

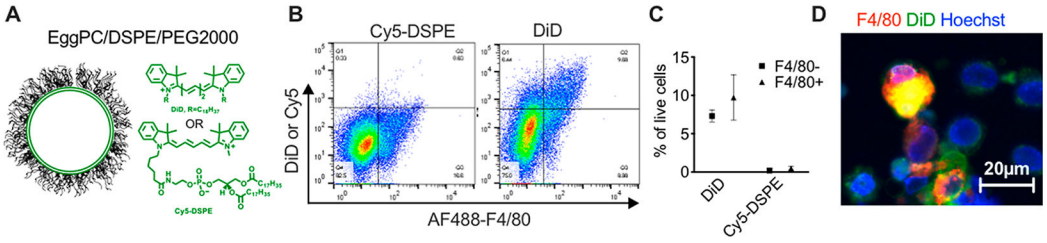

Figure 3.

ICLs but not FPLs label the tumor microenvironment. (A) EPC/DSPE-PEG2000/DiD or EPC/DSPE-PEG2000/Cy5-DSPE liposomes were prepared (Table 1). The probes have the same fluorescent headgroup but different lipid parts. (B, C) 4T1 mice were injected i.v. with DiD or Cy5-DSPE liposomes. Flow cytometry of the tumor single-cell suspension 4 days postinjection shows that about 17% of cells were labeled with DiD and over 50% were F4/80+ macrophages ($n = 3$ mice). (D) Microscopy image of single-cell suspension of tumors after staining for F4/80.

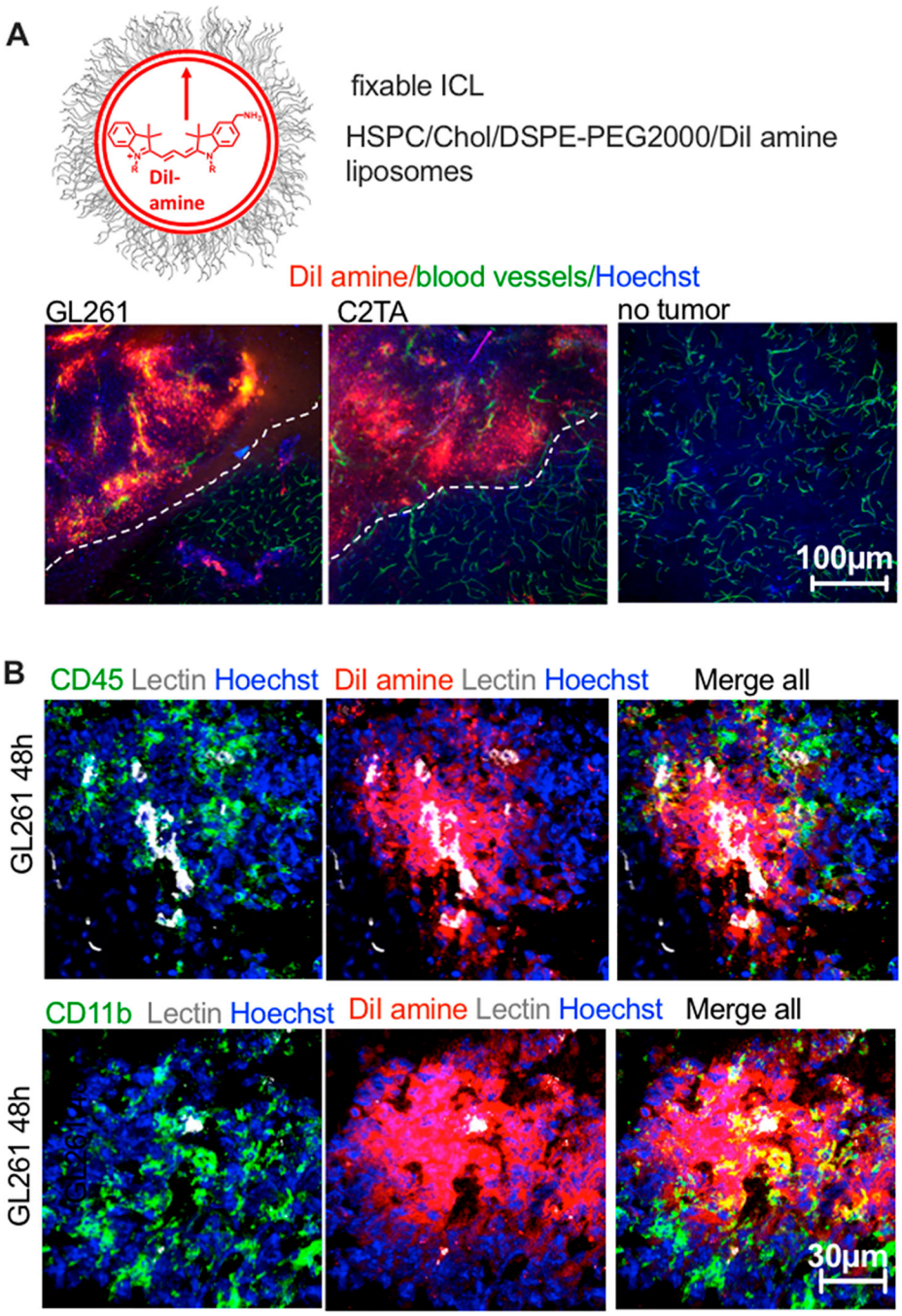

Figure 4.

Extravasation and immune uptake of ICLs in gliomas. (A) amino-DiI (fixable dye) liposomes were injected in GL261 CT-2A syngeneic tumor-bearing mice. Whole brain slices were imaged 48 h thereafter. DiI amine shows efficient extravasation in tumors but not in healthy brain tissue. (B) Tumors were stained for the myeloid marker CD11b and the general immune marker CD45.

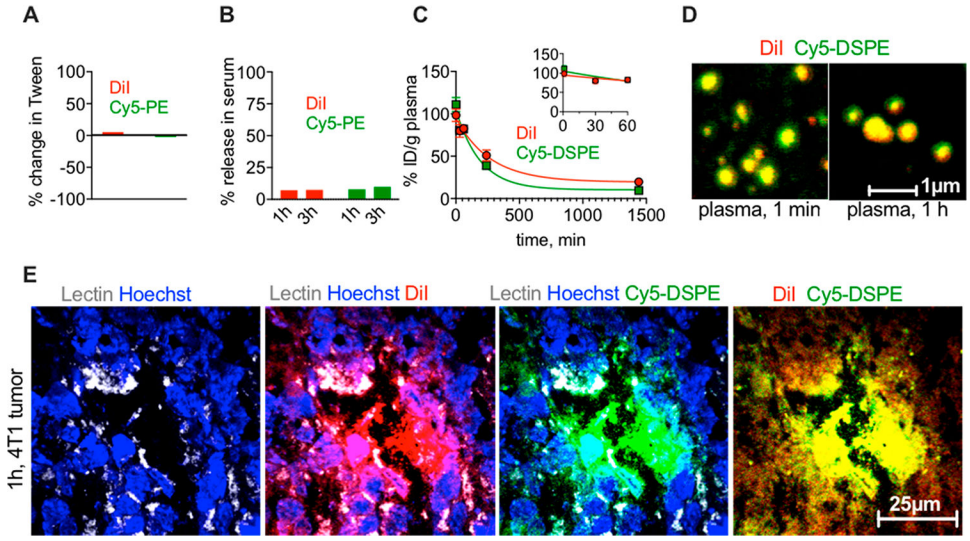

Figure 5.

Both ICL and FPL are stable in serum and extravasate together at early time points. (A) Incubation of EPC/DSPE-PEG2000/DiI/Cy5-DSPE-labeled liposomes in 1% Tween-20 that destroys liposomes does not affect the fluorescence significantly, excluding quenching (repeated twice). (B) There was less than 10% release of DiI and Cy5 fluorescence from liposomes in mouse serum *in vitro* (repeated twice). (C) DiI and Cy5 in plasma after injection of liposomes in 4T1 tumor-bearing mice show similar elimination profile (the inset shows elimination within first 60 min postinjection (n = 3 mice)). Over 99% of fluorescence was in plasma fraction, and no binding to red blood cells was observed (Figure S6). (D) Both lipids are mostly localized in liposomes in plasma that was retrieved from mice at 1 min and 1 h postinjection. Note that the size estimate by confocal microscopy is not accurate, and also the size *in vivo* could be affected by protein corona *etc*. (E) high-magnification confocal microscopy of 4T1 tumor sections at 1 h show that both DiI and Cy5-DSPE are together in lectin-positive blood vessel and extravasate either as intact liposomes or as diffuse fluorescence.

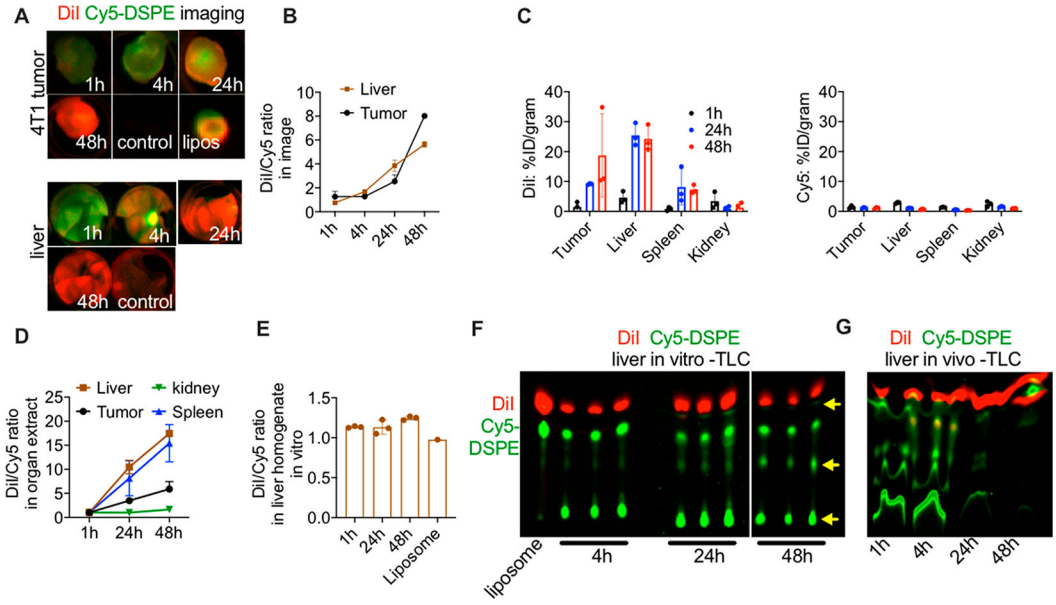

Figure 6.

FPLs are less stable than ICLs and are eliminated from tumor and organs *in vivo*. (A) Mice were injected with DiI/Cy5-DSPE-labeled liposomes, and tumors (upper panel) and livers (lower panel) were excised and imaged at different time points. Representative images of merged DiI and Cy5 fluorescence are shown ($n = 2$ mice, repeated three times). Liposomes were dotted on a membrane and scanned together with tumors (image of the liposomal dot is shown in upper panel). (B) The DiI/Cy5 fluorescence ratio in tumor and liver images shows an increase over time ($n = 2$ mice per time point). (C) Tumors and major organs were homogenized and the lipids were extracted with organic solvent as described in the Methods. DiI (left graph) and Cy5 (right graph) show major differences in biodistribution. (D) The DiI/Cy5 fluorescence ratio in tumor and organ extracts shows an increase over time. (E) Liver homogenates were spiked with DiI/Cy5-DSPE liposomes and incubated for different times. There was no increase in DiI/Cy5 fluorescence ratio over time. (F) Thin layer chromatography analysis of fluorescence after lipid extraction from liver homogenates in (E). The arrow points to degradation of Cy5-DSPE. (G) TLC analysis of liver extracts at different times after injection of DiI/Cy5-DSPE-labeled liposomes shows a decrease in the levels and degradation of Cy5-DSPE but not DiI.

Table 1.

Characterization of Liposomes Used for the Study[a]

liposome compositions	size (intensity weighted), nm	PDI	ζ potential, mV
EPC/DSPE-PEG2000/DiI/Cy5-DSPE 0.2%/0.2%	132	0.167	−20.1
HSPC/Chol/DSPE-PEG2000/DiI/Cy5-DSPE 0.2%/0.2%	150	0.188	−22.7
EPC/DSPE-PEG2000/DiD/Cy3-DSPE 0.2%/0.2%	290	0.287	−18.7
EPC/DSPE-PEG2000/DiD 0.2%	174	0.131	−13.5
EPC/DSPE-PEG2000/Cy5-DSPE 0.2%	158	0.114	−16.3
HSPC/Chol/DSPE-PEG2000/DiI-amine	232	0.218	−17.3

[a]Representative batches are shown. ICLs are DiI, DiD, and DiI-amine. FPLs are Cy3-DSPE and Cy5-DSPE.